

NUMERICAL SIMULATION OF HIGH POWER r.f. SOURCES

A. T. Drobot, L. Seftor, K. Ko
Science Applications, Inc.
1710 Goodridge Drive
McLean, Virginia 22102

and

H. Hanerfeldt, W. B. Herrmannsfeldt
Stanford Linear Accelerator Center
Stanford, California 94305

1.0 INTRODUCTION

In high power microwave tubes the efficient conversion of kinetic electron beam energy to r.f. in a narrow frequency band involves complicated nonlinear electron dynamics and may involve the spontaneous generation of waves at other frequencies. This paper describes the adaptation of an electromagnetic 2D-3V particle-in-cell code MASK to the simulation of such high power r.f. sources. In situations where the r.f. interaction results in the reflection of beam particles, or where there is the excitation of multiple modes internal to the microwave device, simulations are a new tool that permit a representation of the physical processes. In addition, they are capable of modeling the transient behavior and not just steady state operation.

One of the applications of MASK at SLAC is to aid in the design of a new 150 MW Klystron at 2.85 GHz. This work is currently in progress and the approach to it is outlined. Preliminary results have been obtained for a model two cavity problem and are presented. These results illustrate the complicated dynamics in the nonlinear regime including the presence of reflected particles and harmonic generation. The code has also been run in the linear regime where good agreement has been found with small signal theory.

2.0 MASK SIMULATION CODE

Electromagnetic particle-in-cell simulations have been developed by the plasma physics community in the last ten years to study numerable nonlinear problems of beam dynamics, plasma stability, and diode behavior where analytical or simple modeling is difficult¹. The essential formulation is for the time evolution of an initial value problem. The electric and magnetic fields are integrated forward in time from difference forms of the equations

$$\frac{\partial \vec{E}}{\partial t} = c^2 \nabla \times \vec{B} - \vec{J} / \epsilon_0, \quad \frac{\partial \vec{B}}{\partial t} = - \nabla \times \vec{E}, \quad (1) \quad (2)$$

subject to the appropriate boundary conditions. Poisson's equations, $\nabla \cdot \vec{E} = \rho / \epsilon_0$, serves as our initial condition. It is enforced during the integration. The current density \vec{J} and space charge density ρ are attributed onto the mesh from following the orbits of macroparticles which represent a

large number of (in the case of beams) electrons. In turn, the forces acting on a macroparticle can be determined by interpolating the electric and magnetic fields to its position.

The version of MASK applied to the Klystron problem has two spatial dimensions (cylindrical: r-z) and involves the integration of all six field components, TM-(E_r, E_z, B_θ) and TE-(E_θ, B_r, B_z) as well as three velocity components for the macro-particles (V_r, V_z, V_θ). In addition to the numerical representation of the equations the code contains numerous diagnostics.

These include:

- Phase space plots of particle locations.
- Contours of all field quantities.
- Time histories of field behavior at specified locations.
- Energy flow.
- Energy equipartition between field components and particles.
- Reconstruction of particle trajectories.
- Fourier decomposition of the wave spectrum both temporally and spatially.

3.0 APPLICATION TO KLYSTRON DESIGN

In applying MASK to Klystron design the major difficulty encountered has been in the treatment of the drive, idler, and output cavities. The natural timescale for the simulation is on the order of several thousand timesteps or $\sim 1-10$ nsec. The filling time of the cavities is much longer. The important information to be garnered from the code is the voltage and phase of each cavity as well as location for achieving maximum efficiency. We have therefore sought a scheme for imposing the voltage and phase close to what the "equilibrium" solution may be. There are three ways of doing so:

- 1) To treat the full geometry at each cavity and to initiate the simulation with a prefill of r.f. in the desired phase.
- 2) To impose on impedance boundary condition on the drift tube wall corresponding to the cavity structure and to then impose the voltage and phase as a boundary condition.

- 3) Apply the cavity fields by superposition from analytical or numerical calculations of the cavity mode patterns necessitating a numerical representative of the problem in the drift tube.

We have discarded the first approach because it is wasteful. That is, wave properties in empty cavities are well understood and it would take memory space to represent the full cavity as well as the drift region. We are now exploring the two other options.

The input cavity is perhaps the easiest to model because its phase is known and, being in the linear regime, the voltage corresponding to a given drive power is easily determined. The intermediate cavity voltages can be determined from power balance, that is, in "equilibrium", $\int E \cdot J d^3x$ over the region of influence of the cavity must have a time average corresponding to the cavity loss. With the exception of the penultimate cavity this can again be guided by linear theory. In the penultimate cavity an iteration must be used to find the voltage and phase at which power balance is achieved. In the output cavity an iteration must be conducted to determine the phase and voltage at which maximum efficiency occurs. The optimum locations of the cavities can be guessed from the code diagnostics such as the field time histories and current density contours. The eventual problem is still quite difficult because it requires the determination of N sets of parameters, where N is the number of cavities in the Klystron. The sets consist of (L_N, V_N, ϕ_N) , the position, the voltage, and the phase of each cavity.

4.0 RESULTS FOR THE TWO CAVITY KLYSTRON

The initial calculations performed with the code on the SLAC IBM3081 have been of beam bunching in an idealized two cavity klystron. An electron beam was injected into a drift tube with radius $r_w = 1.35$ cm and filled to a radius $r_b = 1.0$ with a uniform density profile. The beam parameters were $V_0 = 80$ KV and $I_0 = 48.3$ amps. The background guide magnetic field $B_{z0} = .135$ Tesla. In these simulations the beam injection boundary was fixed at zero potential as was the boundary at the output end. The simulation was performed on a 128×27 mesh with $\Delta z = .09$ cm and $\Delta R = .05$ cm. The time-step chosen was 8.75×10^{-13} sec which corresponded to 400 timesteps per cycle of the drive wave at 2.85 GHz. The first set of studies was for beam bunching by the drive cavity operating at various voltages. This cavity was centered 3.0 cm away from the beam injection plane and had a gap width of 0.63 cm opening onto the drift tube. Figure 1 shows the response of the beam particle momentum as a function of axial distance for various applied voltages in the driving gap. These phase space plots were all taken at the same phase relative to the drive field at times when the transient response had died out. The case of zero drive voltage is included for comparison.

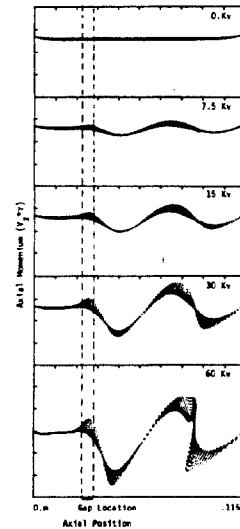


Fig. 1. Bunching caused by drive cavity for various applied gap voltages, as seen in phase space.

It shows no perturbation other than the space charge depression at the injection and output ends. The cases of 7.5 KV and 15.0 KV correspond to the linear theory for a cold beam with axial motion only. The diagnostics indicate that the E_z Field component for these two cases has a simple sinusoidal time dependence at the drive frequency. In contrast the 30 KV case exhibits some nonlinear behavior while at 60 KV particle trapping can be seen and it is also evident that waves have propagated back upstream. The wavelength of the space charge waves for drive voltages at 30 KV and below is in excellent agreement with linear theory. The 60 KV this is only approximately true.

We chose to examine the 30 KV case in some detail and to use that as the drive voltage for the two cavity study. The reason was that good spatial bunching was observed without the generation of spurious modes above the cutoff in the drift tube. In Figure 2 the phase space for the 30 KV case is shown as a function of time in increments of a tenth of a wave period.

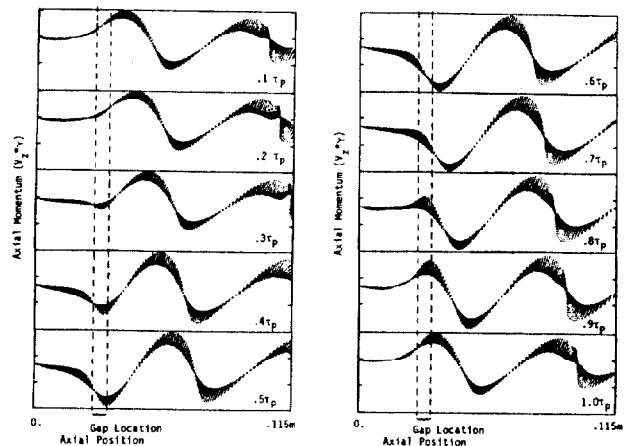


Fig. 2. Electron dynamics in phase space as a function of time for 30 KV drive on the first gap. t_p is the wave period. (Note: due to automatic scaling the vertical scale varies very slightly between plots.)

Using the information in Figure 2 it is possible to deduce the phase velocity of the space charge wave by following the advance of crests in the velocity perturbation. The result is again in excellent agreement with linear theory.

The composite in Figure 3 shows the density and velocity perturbation for the 30 KV case at a point in time when the space charge bunch is passing the location of what will be the output cavity.

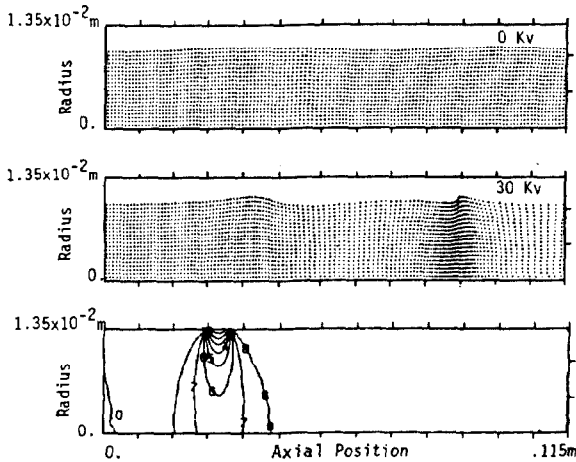


Fig. 3 Bunching in space and contour of axial driving (E_z) electric field.

For contrast the density plot for the undisturbed beam is also shown. A contour of the driving electric field, E_z , is also shown on the figure. As can be seen quite plainly, the particles at larger radius are more strongly influenced and hence more tightly bunched. The induced electric field at the location of the output cavity is shown in Figure 4 as a function of time.

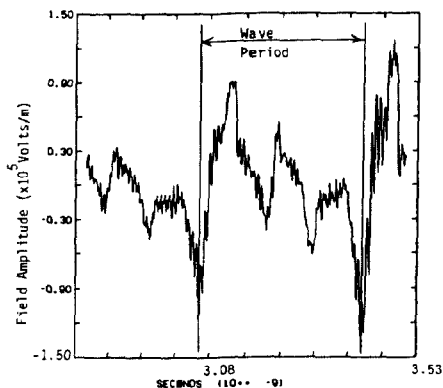


Fig. 4 Probe signal from 30 KV drive indicating strong generator of the third harmonic.

There is no longer a simple sinusoidal variation as for the lower voltage cases. A strong third harmonic is generated, but its frequency is still below the cutoff for the drift tube. At 60 KV higher harmonics are excited and travel back upstream.

To begin the iteration process for determining the parameters of the output cavity, located at $z \cong 8.5$ cm, we chose a

voltage of 90 KV and a phase of -90° . The choice of phase was dictated by linear theory for the 30 KV case and corresponded to the phase when the beam bunch passed the output cavity as can be deduced from Figures 2 and 3. The resulting efficiency was $\sim 4\%$. We have found that the initial voltage chosen was probably too high and that it resulted in strong particle trapping and particle reflection as shown in Figure 5.

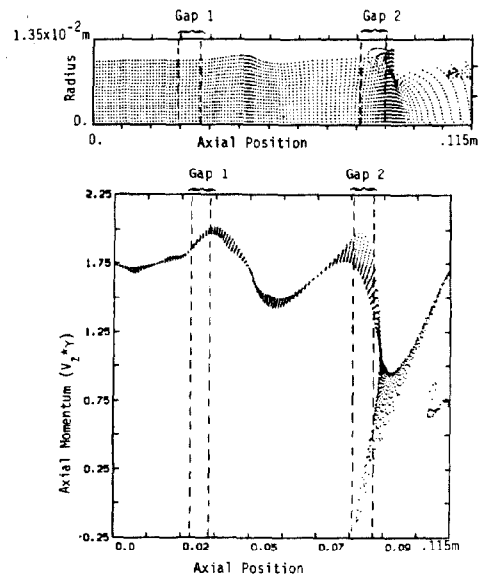


Fig. 5 Particle dynamics in the presence of an output cavity at 90 KV and a phase of -90° .

Again wave propagation from higher harmonics in the upstream direction was observed. The presence of the output cavity retarded the velocity of the space charge bunch significantly. We have at this stage lowered the output voltage to 80 KV and tried phases of -100° and -80° . These yielded efficiencies of 8% and $>1\%$ respectively. Further work is still in progress.

ACKNOWLEDGMENTS

We would like to thank Dr. Dave Sutter and Stan Staton of DOE for making possible the use of the MFE computing center. We further acknowledge useful discussions with Dale Nielson of LLNL, Carl Bane and G. Konrad of SLAC.

This work was performed under contract 515-PS-139.

REFERENCES

1. A. Bruce Langdon and Barbara F. Lasinski, in *Methods in Computational Physics* Vol. 16, Academic Press, 1976, p. 327-366.